




## PAPER

View Article Online  
View Journal | View Issue



Cite this: *Environ. Sci.: Atmos.*, 2023, 3, 374

# Chemical characterization of aerosols in the South Asian outflow over the northern Indian Ocean: latitudinal gradients and ultrafine particle events†

Vijayakumar S. Nair, <sup>a</sup> S. Suresh Babu,<sup>a</sup> Sobhan Kumar Kompalli, <sup>a</sup> V. Jayachandran, <sup>b</sup> T. C. Ajith<sup>a</sup> and Mukunda M. Gogoi<sup>a</sup>

Chemical properties of the continental outflow to the northern Indian Ocean are investigated using shipborne measurements carried out as a part of the Integrated Campaign for Aerosols, gases and Radiation Budget (ICARB-2018) experiment during winter 2018. The organic carbon (OC) and elemental carbon (EC) showed high values ( $OC = 4.8 \pm 2.1 \mu g m^{-3}$  and  $EC = 2.0 \pm 0.6 \mu g m^{-3}$ ) over the northern Indian Ocean and relatively lower values ( $OC = 1.20 \pm 0.50 \mu g m^{-3}$  and  $EC = 0.82 \pm 0.53 \mu g m^{-3}$ ) over the equatorial Indian Ocean. The relative contribution of organic matter (OM) to the sub-micron mass loading also decreased from southeastern Arabian Sea (40%) to the equatorial Indian Ocean (23%). The short-term increase in OC, the OC/EC ratio, OM and the OM/sulfate ratio during ultrafine particle bursts over the remote equatorial Indian Ocean indicate the possibility of prominent sources of marine organic compounds. In the southeastern Arabian Sea, the mass concentration of all aerosol species showed a decreasing trend towards the open ocean, where the magnitude of this latitudinal decrease was relatively higher for OC and OM compared to EC and sulfate. The latitudinal variation in the OM/sulfate ratio showed a reduction from  $1.20 \pm 0.11$  to  $0.47 \pm 0.15$ , which is further supported by the similar latitudinal decrease in the OC/EC ratio. These observations indicate the possible loss of organic aerosols, which might be due to ageing during long-range transport. The synthesis of earlier measurements over South Asia and surrounding oceanic regions also shows a relative decrease in the organic mass concentration, which changes the organics-rich nature of the South Asian aerosol system during transport.

Received 3rd October 2022  
Accepted 5th December 2022

DOI: 10.1039/d2ea00130f

rsc.li/esatmospheres

## Environmental significance

The outflow of anthropogenic particles from South Asia to the northern Indian Ocean is a major scientific concern during winter. In this study, shipborne measurements are used to investigate the change in aerosol composition, especially organics, during short-term ultrafine particle events. The origin of these ultrafine organic aerosols over the equatorial Indian Ocean remains an open question. Furthermore, organics decrease at a faster rate towards the open ocean than all other aerosol species, which indicates the loss of organics due to the ageing process during long-range transport, transforming the organics-dominated outflow into a sulfate-dominated aerosol system over the far oceanic regions.

## 1 Introduction

South Asia is considered one of the major hotspots of aerosols and trace gases, especially during winter.<sup>1–3</sup> Extensive measurements from various locations across South Asia indicated a significant dominance of carbonaceous aerosols (>50%) in the mass loading of fine mode (<1  $\mu m$ ) particles during winter.<sup>2,4–6</sup> The regional circulation favours the transport of these continental aerosols to the Bay of Bengal and Arabian Sea

(northern Indian Ocean), which raises serious concerns because of the direct and indirect radiative forcing due to aerosols, and also due to its role in nutrient transport and ocean biogeochemistry.<sup>3,7–9</sup> High concentrations of carbonaceous aerosols (especially black carbon or elemental carbon) were observed over the northern Indian Ocean, which is mostly transported from South Asia and Southeast Asia, as reported by earlier campaigns such as the Indian Ocean Experiment (INDOEX-1999) and Integrated Campaign for Aerosols, gases and Radiation Budget (ICARB 2006 and 2009) over this region.<sup>3,10,11</sup> Though several studies investigated the chemical characteristics of aerosols during different air masses over the northern Indian Ocean, short-term variations and chemical evolution of the South Asian outflow were not investigated in detail.<sup>12</sup> This knowledge gap is mostly attributed to the poor

<sup>a</sup>Space Physics Laboratory, Vikram Sarabhai Space Centre, Thiruvananthapuram, India. E-mail: vijayakumarsnair@gmail.com

<sup>b</sup>National Atmospheric Research Laboratory, Department of Space, Tirupati, India

† Electronic supplementary information (ESI) available. See DOI: <https://doi.org/10.1039/d2ea00130f>



spatial and temporal resolution of aerosol chemical composition measurements over the region,<sup>7–10,13–15</sup> which hinders the understanding of the chemical processing of aerosols at shorter time scales.

Organic aerosols dominate the total aerosol loading over the South Asian region. The secondary organic aerosols (SOA) mostly formed from low or semi-volatile organic compounds account for the major portion of the fine particulate mass loading.<sup>16</sup> Nucleation and condensation of organic vapours on existing particles significantly contribute to the mass loading and higher growth rate of ultrafine particles,<sup>17,18</sup> which remains largely unexplored in the South Asian region. Addressing the formation, evaporation, gas-phase photo-oxidation, condensational growth and phase state of organics is far more complex than those of the chemically inert black carbon or elemental carbon.<sup>19</sup> Several laboratory-based (chamber) and modeling studies have investigated the evolution of organic aerosols in the atmosphere; still, uncertainties persist due to a large number of compounds that need to be considered.<sup>20–23</sup> In contrast to the secondary formation pathway of sulfate, organic compounds have a wide range of volatility and heterogeneous pathways, making it difficult to predict the concentration of secondary organics accurately.

Over marine (receptor) environments, aerosol composition and size distribution are highly influenced by transport efficiency of aerosols, and the mixing state and photochemical ageing during transport. The mixing of continental and marine air masses results in significant changes in the physiochemical properties and atmospheric lifetime of aerosols.<sup>20</sup> Hence, the formation and removal of aerosols over the outflow regions assume importance for the estimation of the aerosol mass budget and thus climate impact assessments. In this background, extensive measurements of aerosols in the South Asian outflow over the northern Indian Ocean were carried out during ICARB-2018 (January–February 2018) to study the change in the aerosol composition over the source (land) and receptor (ocean) regions. The objectives of this study include the characterization of chemical properties of aerosols over the Indian Ocean during the South Asian outflow, and its latitudinal variations and chemical evolution during long-range transport. In this paper, we describe the high-resolution measurements of the radiatively important fine mode aerosol composition (non-refractory and carbonaceous) and the change in chemical composition during ultrafine particle events and because of long-range transport.

## 2 Experimental details and methodology

The ICARB-2018 experiment was carried out onboard the Oceanographic Research Vessel Sagar Kanya from 16 January to 13 February 2018 (winter season), covering the northern and equatorial Indian Ocean (15° N to 2° S and longitudes 65° E to 76° E). The cruise track of the ICARB-2018 is shown in Fig. 1. The latitudinal transect across the South Asian outflow is called

phase 1, and the longitudinal transect over the equatorial Indian Ocean (~2° S) is called phase 2.

Calm and hazy sky conditions prevailed over the northern Indian Ocean during ICARB-2018. The *in situ* measurements of meteorological variables indicate that winds were mostly northeasterly during phase 1 and northerly or northwesterly during phase 2. The average wind speed increased from 2.9 m s<sup>-1</sup> to 4.7 m s<sup>-1</sup> over the phases 1 and 2 regions, respectively. The average temperature and relative humidity during phase 1 (27.7 ± 0.6 °C and 73.1 ± 5.0%) and phase 2 (28.2 ± 0.5 °C and 72.8 ± 3.5%) of the campaign were comparable and both periods were devoid of major weather systems. During the return leg of the experiment, large-scale rainfall was observed on 4, 6 and 7 February over the northern Arabian Sea and Indian subcontinent. This widespread rainfall associated with the western disturbances modified the large-scale meteorology and aerosol properties over the region. Hence, the data collected after 4 February, 2018 were not considered for further analysis. More details of measurements, sampling protocol, meteorology and air mass back trajectory analysis during ICARB-2018 are available elsewhere.<sup>13,24</sup>

Five-day air mass back trajectories reaching the cruise track on each day are estimated (Fig. 1d–f) using the Hybrid Single-Particle Lagrangian Integrated Trajectory (HYSPPLIT) model and the schematic of the mean air mass pathways is shown in Fig. 1b. The phase 1 region was directly under the influence of continental outflow as the air mass back-trajectories originated from peninsular India or the Bay of Bengal (Fig. 1d), whereas the air mass back trajectories were mostly confined within the northeastern Arabian Sea, without the direct influence of continental sources, during the second phase over the equatorial Indian Ocean (Fig. 1e).

A customized aerosol laboratory was set up at the top deck (~15 m above the mean sea level) of the ship, and ambient air was aspirated into the laboratory using iso-kinetic community inlets at a flow rate of 16.6 litres per minute (LPM). The measurements of aerosol chemical composition using the aerosol chemical speciation monitor (ACSM), mass concentrations of organic carbon (OC) and elemental carbon (EC) using a semi-continuous aerosol carbon analyzer and aerosol size distribution using a scanning mobility particle sizer (SMPS) form the major dataset for this study.

### 2.1 ACSM

The mass concentration of sub-micron non-refractory aerosols (NR-PM<sub>1.0</sub>) measured using the ACSM instrument (Make: Aerodyne, USA) includes organic matter (OM), sulfate, nitrate, ammonium, and chloride. Measurements were carried out at 30 minute (near real-time) intervals. A sample flow of 0.1 LPM, through a critical aperture with a fixed diameter (100 µm), was drawn from the main aerosol inlet system having a flow rate of 3 LPM for near isokinetic sampling conditions. Before the experiment, the instrument was calibrated for its ionization efficiency (IE) and relative IE (RIE) by using monodisperse (300 nm) particles of NH<sub>4</sub>NO<sub>3</sub> and (NH<sub>4</sub>)<sub>2</sub>SO<sub>4</sub> following the standard calibration procedure suggested in the literature.<sup>25–27</sup> The



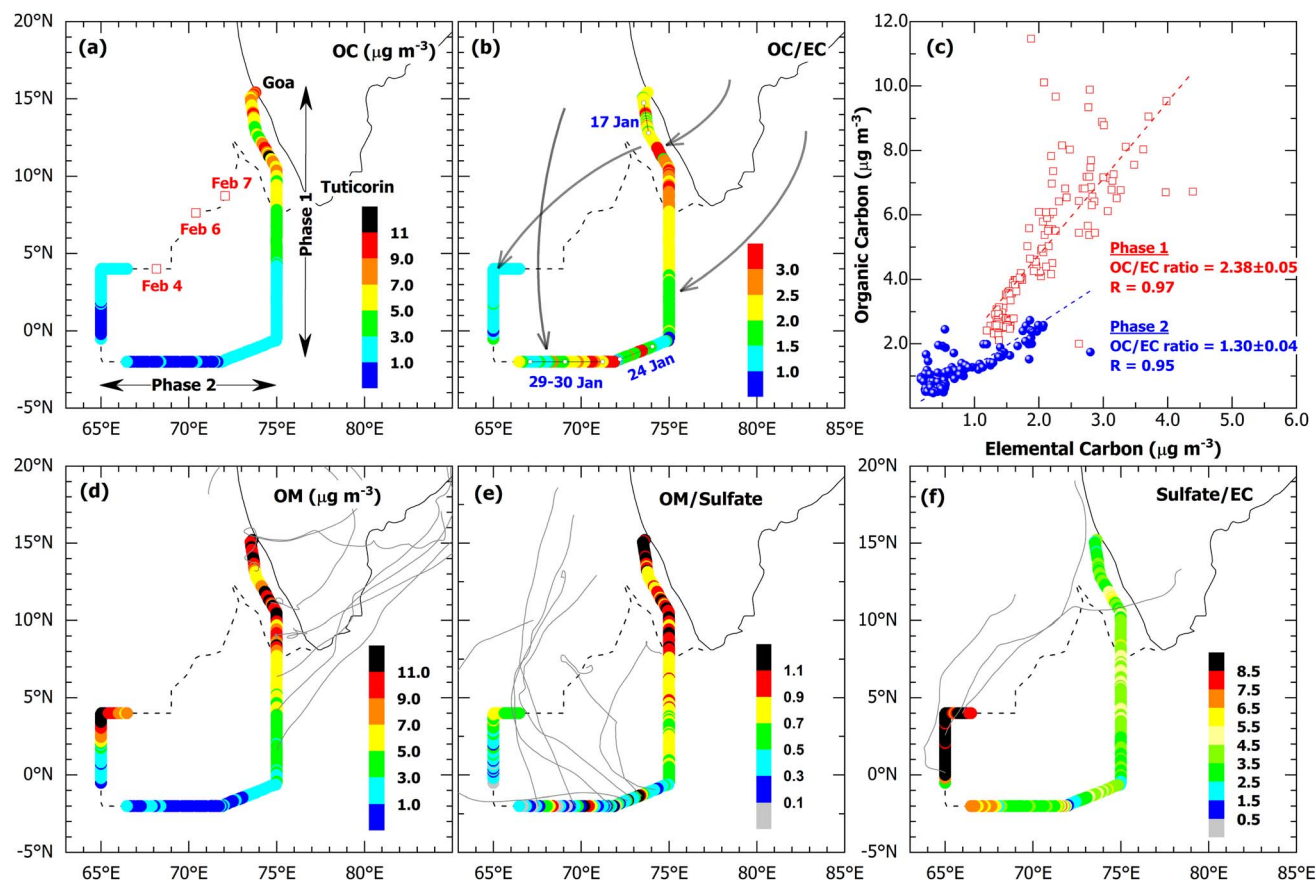


**Fig. 1** (a) Mass concentrations of organic carbon (OC,  $\mu\text{g m}^{-3}$ ), (b) ratio of OC to elemental carbon (EC,  $\mu\text{g m}^{-3}$ ), (d) mass loading of organic matter (OM,  $\mu\text{g m}^{-3}$ ), (e) ratio of OM/sulfate and (f) ratio of sulfate to EC along the cruise track over the northern Indian Ocean during 16 January 2018 to 13 February 2018. (c) Scatter diagram showing the OC and EC mass concentrations during the first and second phases of ICARB-2018. The cruise track is represented by dashed lines. Rainy days are marked as 04Feb, 06Feb, and 07Feb indicating 4, 6, and 7 February 2018. We have not considered the measurements made during the return segment of the cruise because of the rain events and changes in the weather system. Thick solid arrows on panel (b) schematically represent the air mass pattern over the measurement region and continuous grey lines in (d)–(f) are air mass trajectories estimated using the HYSPLIT model.

response factors were determined by comparing the response factors of the ACSM to the mass calculated with a known particle size (300 nm; selected using an electrostatic classifier – TSI 3080 with a long differential mobility analyser) and the varying number concentrations ( $\sim 50$ – $2000 \text{ cm}^{-3}$ ) as measured by using a condensation particle counter (CPC, TSI 3786). We have used a default RIE value of 1.4 for OM.<sup>25,28</sup> The corrections required for the instrument performance for the varying inlet pressures and  $\text{N}_2$  signal (*i.e.*, air-beam correction required for normalizing the measurements with respect to drifts in measurement sensitivity and the sampling flow rate) were carried out during this study.<sup>28,29</sup> Furthermore, we have used the signals from an internal diffuse naphthalene source ( $m/z$  128) for correcting the mass-dependent ion transmission efficiency of the residual gas analyser. Both  $\text{N}_2$  and naphthalene signals were also used for the determination of the relative ion transmission (RIT) efficiency. The measured fractions of unit mass resolution spectrum signals were apportioned to individual aerosol species by using the default fragmentation table. Since the present ACSM consists of a capture vaporizer that results in a higher collection efficiency (about unity),<sup>30</sup> we have not

applied the composition-dependent collection efficiency correction while processing the data. Reproducibility uncertainty of NR-PM1.0, nitrate, organic matter, sulfate and ammonium was 9%, 15%, 19%, 28%, 36% respectively.<sup>26</sup> A good association between the ACSM and HR-ToF-AMS for  $\text{NO}_3$  (slope = 1.14,  $R^2 = 0.99$ ),  $\text{SO}_4$  (slope = 0.954,  $R^2 = 0.93$ ) and  $\text{NH}_4$  (slope = 13.2,  $R^2 = 0.88$ ) was also reported during the ACSM inter-comparison experiment.<sup>26</sup>

## 2.2 Semi-continuous aerosol carbon analyser

The simultaneous measurements of mass concentrations of the EC and OC were carried out using a semi-continuous aerosol carbon analyser (Make: Sunset Laboratories, USA).<sup>31</sup> Ambient aerosols collected on a quartz fibre filter were exposed to an increasing temperature ramp following the NIOSH 5040 (National Institute for Occupational Safety and Health) protocol inside an oven purged with inert helium gas. Continuous monitoring of absorbance using a diode laser is used to correct the uncertainties in OC and EC measurements.<sup>32</sup> The relative standard uncertainty for OC and EC was 12% and 18%



respectively.<sup>33</sup> During ICARB-2018, ambient air was sampled through a dedicated inlet system having an inertial impactor with a particle size cut off at  $2.5\ \mu\text{m}$  at a flow rate of 8.0 LPM onto a quartz fiber filter with a 1.6 cm diameter. Nafion membrane tubes are used to maintain the relative humidity of the sample at 50% and annular denuders were used to remove the volatile organic gases from the air sample. We have used a known amount of aqueous sucrose solution (99.5% from Sigma Aldrich) to ensure the calibration consistency of the instrument. The measurement bias was estimated from the measured and injected amount of carbon, which was less than 6% during the experiment. The limit of detection for OC and EC using the semi-continuous OCEC analyzer was  $0.1\ \mu\text{g m}^{-3}$  and  $0.01\ \mu\text{g m}^{-3}$  respectively.<sup>32</sup>

### 2.3 SMPS

The aerosol number size distributions (NSD) for the size range from  $\sim 9$  to  $420\ \text{nm}$  were measured using a scanning mobility particle sizer (SMPS, Make: TSI) at every 3 minutes interval. The SMPS consists of a differential mobility analyser (DMA, TSI 3081), which segregates the aerosols according to their electrical mobility. These mono-dispersed aerosols are fed to a water-based condensation particle counter (CPC, TSI 3786), where they are allowed to grow to the optically detectable size range. These particles are counted by using an optical particle counter.<sup>34</sup> Uncertainties in SMPS due to flow and charging efficiency are 2% and  $\pm 10\%$  respectively. The instrument-specific corrections were applied to all the measurements and

then averaged and geolocated hourly using global positioning system (GPS) data.

We have compiled the earlier measurements of aerosol chemical composition over distinct environments in the Indian landmass and the shipborne measurements carried out during the INDOEX-1999, ICARB 2006, WICARB 2009 (Winter Phase of ICARB) and ARMEX (Arabian Sea Monsoon Experiment) as ESI.<sup>†</sup> The majority of studies reported OC values (using the thermal-optic technique) over the Indian region and the direct measurements of OM are limited.<sup>4,6,35–37</sup> To compare these earlier measurements over the Indian region with ICARB-2018, we have converted the OC values from the literature to OM by using a conversion factor of 1.7. Though the contribution of OC to OM varies depending upon the ageing and extent of the oxidation, we have used an OM/OC ratio of 1.7 to convert the OC measurements to OM.<sup>10,38,39</sup> This conversion factor is applied only to the OC measurements adopted from the literature. It should be noted that the measured OC values over the Indian subcontinent are much higher than the sulfate loading (OC/sulfate ratio  $\sim 2$ ), and hence the assumption of an OM/OC ratio of 1.7 does not influence the findings of this study.

## 3 Results and discussion

### 3.1 Spatial variation of EC, OC, OM and sulfate

The spatial variation of the OC mass concentration measured during ICARB-2018 is shown in Fig. 1a. The time series of aerosol properties measured during ICARB-2018 are shown in

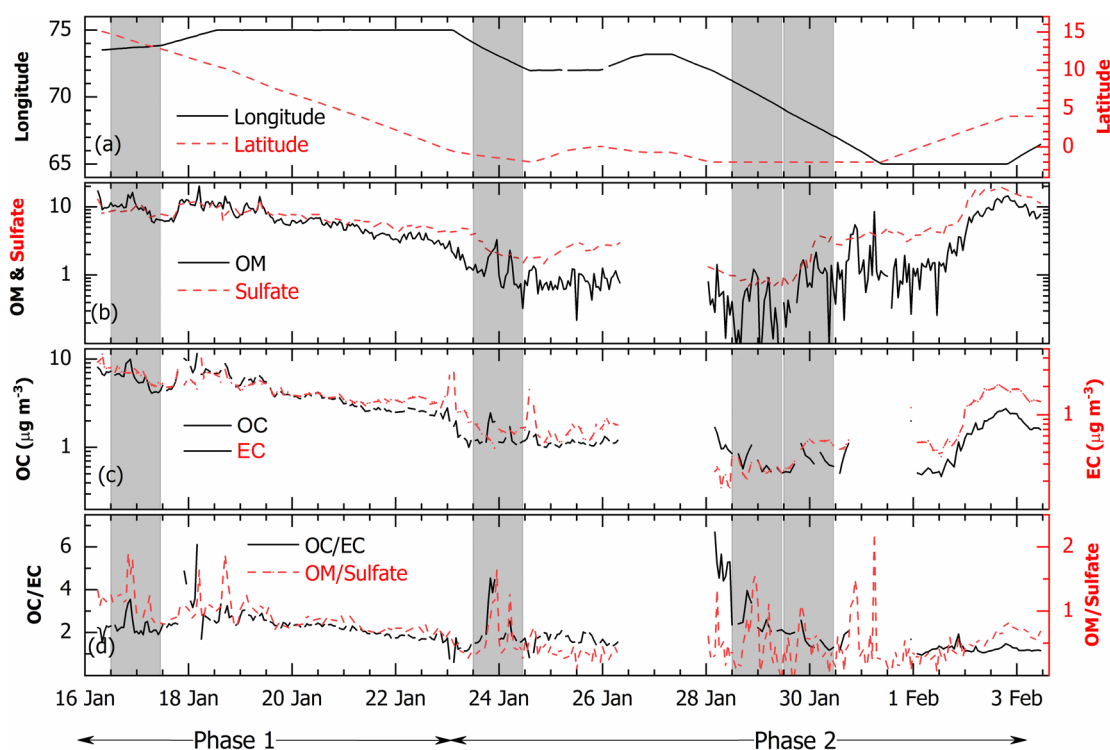


Fig. 2 Time series of (a) latitude and longitude of the cruise track, (b) mass concentration of organic matter (OM) and sulfate, (c) mass concentration of organic carbon (OC) and elemental carbon (EC), and (d) the OC/EC ratio and the OM/sulfate ratio. The ultrafine particle (UFP) event days are identified by the shaded regions.





Fig. 2. The near-real-time (hourly) and spatially resolved measurements indicate high values of OC ( $4.8 \pm 2.1 \mu\text{g m}^{-3}$ ) and EC ( $2.0 \pm 0.6 \mu\text{g m}^{-3}$ ) during the first phase and relatively lower values (OC =  $1.20 \pm 0.50 \mu\text{g m}^{-3}$  and EC =  $0.82 \pm 0.53 \mu\text{g m}^{-3}$ ) during the second phase of the campaign. Over the equatorial Indian Ocean, far away (1000 km) from the Indian subcontinent, EC values were as high as  $\sim 1 \mu\text{g m}^{-3}$  and only less than 10% of the total EC values were below  $0.5 \mu\text{g m}^{-3}$  during the campaign. These values are higher than most of the open ocean values reported in the literature. Considering EC as a proxy for combustion-derived aerosols, high EC values near the equatorial Indian Ocean indicate a large-scale influence of the South Asian outflow over the northern Indian Ocean.

The OC/EC ratio gradually decreased towards the equatorial Indian Ocean (Fig. 1b) and the mean values of the OC/EC ratio during phase 1 and phase 2 are  $2.38 \pm 0.05$  and  $1.30 \pm 0.04$  respectively (Fig. 1c). Low values of the OC/EC ratio are mostly seen over the southwestern part of the cruise (Fig. 1f), which is far away from the source regions, and five-day air mass back trajectories were mostly marine. The OM mass concentrations during ICARB-2018 are shown in Fig. 1d. The aerosol mass concentrations decreased gradually as we move away from the continent towards the equatorial Indian Ocean. The contribution of organic matter to the total NR-PM<sub>1.0</sub> decreased from 40% over the southeastern Arabian Sea to 23% over the equatorial Indian Ocean, whereas the sulfate contribution increased from 37% to 49%. The total aerosol mass concentration (NR-PM<sub>1.0</sub>) was highest over the southeastern Arabian Sea ( $23.44 \pm 5.07 \mu\text{g m}^{-3}$ ) due to its proximity to the emission sources on land. Near the coastal regions, concentrations of sulfate and OM are comparable and range between 8 and  $15 \mu\text{g m}^{-3}$ , whereas sulfate aerosols (ranged between 4 and  $8 \mu\text{g m}^{-3}$ ) completely dominated the NR-PM<sub>1.0</sub> mass over the equatorial Indian Ocean, followed by OM ( $2\text{--}6 \mu\text{g m}^{-3}$ ) and ammonium ( $2\text{--}4 \mu\text{g m}^{-3}$ ). There is a reduction in the OM/sulfate ratio between near (OM/sulfate  $\sim 1.0$ ) and far (OM/sulfate  $\sim 0.4$ ) oceanic regions in the downwind of the South Asian outflow (Fig. 1 and 2). The sulfate/EC ratio (Fig. 1f) showed an almost constant value (ranging between 2 and 4) except for the southwestern part of the cruise track (sulfate/EC > 5), where chlorophyll concentrations were also high.<sup>24</sup> Since most of the anthropogenic species did not show an increase over the western Arabian Sea, the increase in the sulfate/EC ratio could be attributed to the secondary formation of sulfate from the oceanic emission of precursor gases or the subsidence of sulfate aerosols formed in the free troposphere to the marine boundary layer.<sup>40</sup>

Several studies have reported high values (2 to  $25 \mu\text{g m}^{-3}$ ) of carbonaceous aerosols (EC or black carbon, OC) over South Asia during the winter season.<sup>2,6</sup> The OC values reported onboard aircraft ( $3.0 \mu\text{g m}^{-3}$ ) and ships ( $0.81 \mu\text{g m}^{-3}$ ) during INDOEX<sup>10</sup> for the marine atmospheric boundary layer are lower than the those in ICARB-2018 measurements. The EC values observed near the Maldives islands during ICARB-2018 are in the range of  $0.5\text{--}1.5 \mu\text{g m}^{-3}$ , which is consistent with the earlier observations from Hanimaadhoo (EC  $\sim 0.59 \pm 0.28$  and OC  $\sim 1.22 \pm 0.71 \mu\text{g m}^{-3}$ ) during November 2014 to April 2015.<sup>7</sup> The high values of EC over the equatorial Indian Ocean further support the higher

transport efficiency of EC during winter.<sup>41</sup> The OC/EC ratio over the equatorial Indian Ocean was lower compared to that of the southeastern Arabian Sea, which indicates the limited spatial coverage of OC compared to EC due to the depletion of OC during transport. The OC/EC ratio (0.5 to 1.5) measured during INDOEX<sup>10</sup> was comparable to the phase 2 value ( $1.3 \pm 0.04$ ) but lower than the phase 1 value ( $2.38 \pm 0.05$ ) during ICARB-2018. Based on measurements over the Bay of Bengal during ICARB-2009, a mean OC/EC ratio of  $3.4 \pm 1.1$  for the wintertime outflow from the Indo Gangetic Plain was reported.<sup>9</sup> Though the equatorial Indian Ocean experiences air masses from the Bay of Bengal region, the OC/EC ratio is significantly lower than the values reported by the earlier studies.<sup>9</sup> The OC/EC ratios reported from the Maldives Climate Observatory – Hanimaadhoo (MCOH) in the equatorial Indian Ocean are very close to those in the ICARB-2018 measurements.<sup>7,12</sup>

Organic aerosols have primary and secondary sources. The volatile organic compounds (VOCs) from both marine and transported-anthropogenic sources get oxidized to less-volatile compounds which can directly partition into the aerosol phase *via* aqueous phase and heterogeneous processes. Over remote oceans, primary emission of water insoluble organics (marine hydrocarbon-like organic aerosols) is also reported.<sup>42</sup> The fractional contribution of water-soluble organic carbon (WSOC) to the total OC was 0.81 and 0.61 over the southeastern Arabian Sea and equatorial Indian Ocean during ICARB-2018.<sup>43</sup> The high contribution of WSOC to OC indicates the role of ageing during long-range transport. Interestingly, sporadic events with high values of OM/sulfate and OC/EC ratios were also observed over the equatorial Indian Ocean during phase 2 (Fig. 1b and e). Though the aerosol mass loading and mean values of OM/sulfate and OC/EC ratios are lower over the equatorial Indian Ocean, the short-term events having a relative increase in OM (and OC) compared to sulfate and EC mass loading were not reported earlier over this region. This aspect is discussed in Section 3.2.

### 3.2 Influence of particle burst on aerosol composition

It is interesting to note that, short-term events with high values of OC/EC ratios were observed over the equatorial Indian Ocean (Fig. 1b and e), though aerosol loading and the mean OC/EC ratio were lower over this region. To investigate this aspect in detail, all 19 days (phases 1 and 2) of ICARB-2018 data were examined and diurnal variations of OC and EC during four days (17, 24, 29, and 30 January 2018), when OC/EC ratio showed short-term events, are shown in Fig. 3. During these event days, the OC mass concentration showed high values for 2 to 3 hours in the early morning (07:00–10:00) and evening (15:00–17:00) hours, whereas simultaneous measurements of EC did not show variations similar to that of OC during these events. Since EC is widely used as a proxy for anthropogenic and biomass burning sources and is co-emitted with OC during combustion, we have ruled out the possibilities of local anthropogenic sources including ship exhaust, or a change in the air mass pattern directly influencing the observed increase in OC.



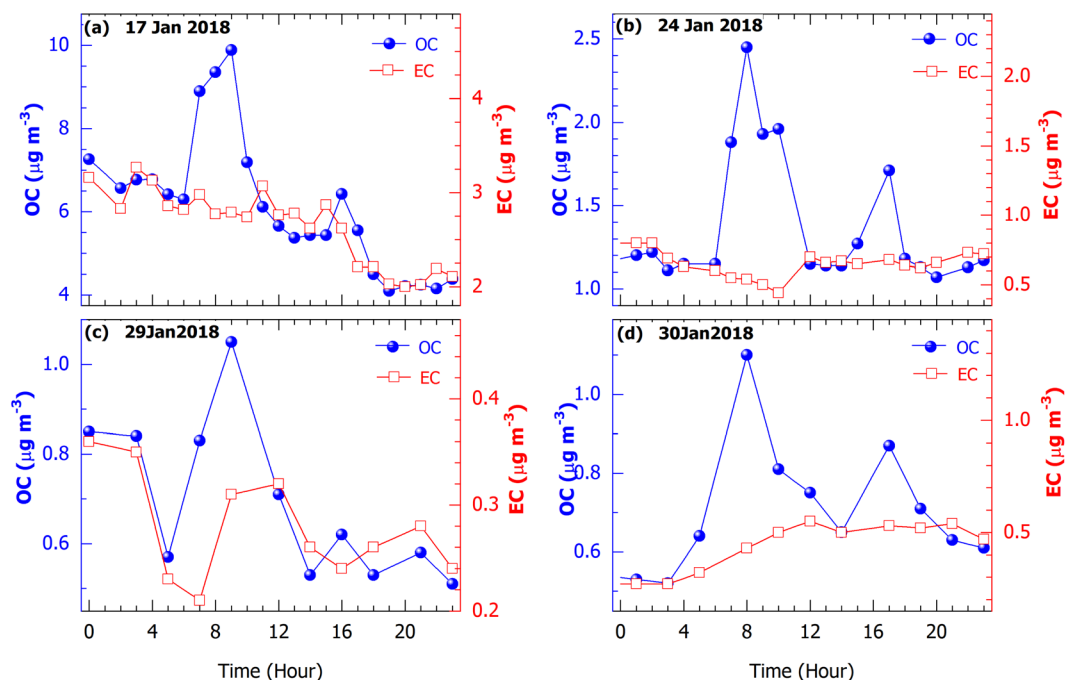


Fig. 3 Diurnal variation of OC and EC mass concentrations ( $\mu\text{g m}^{-3}$ ) during (a) 17 January, (b) 24 January, (c) 29 January and (d) 30 January 2018.

Further analysis revealed that these events are coinciding with ultrafine particle bursts observed in the aerosol number size distribution measurements. The diurnal variation of the OC/EC ratio and geometric mean diameter (GMD) estimated from the aerosol number size distribution for the event days are shown in Fig. 4. The low GMD values over the southeastern Arabian Sea and the equatorial Indian Ocean indicate ultrafine particle events. Most of these events occurred during the early morning and evening hours: the former being more prominent

than the latter. The OC mass loading increased when the GMD decreased significantly. The latitudinal gradient of the OC/EC ratio and its association with GMD is shown in Fig. 5. A systematic decrease in the OC/EC ratio from 3 to 1.75 was observed over the oceanic regions south of Indian peninsula. It is interesting to note that ultrafine particle events were not observed over this region and GMD values were mostly greater than 100 nm. However, the OC/EC ratio varies significantly over the near-coastal and the equatorial Indian Ocean due to the

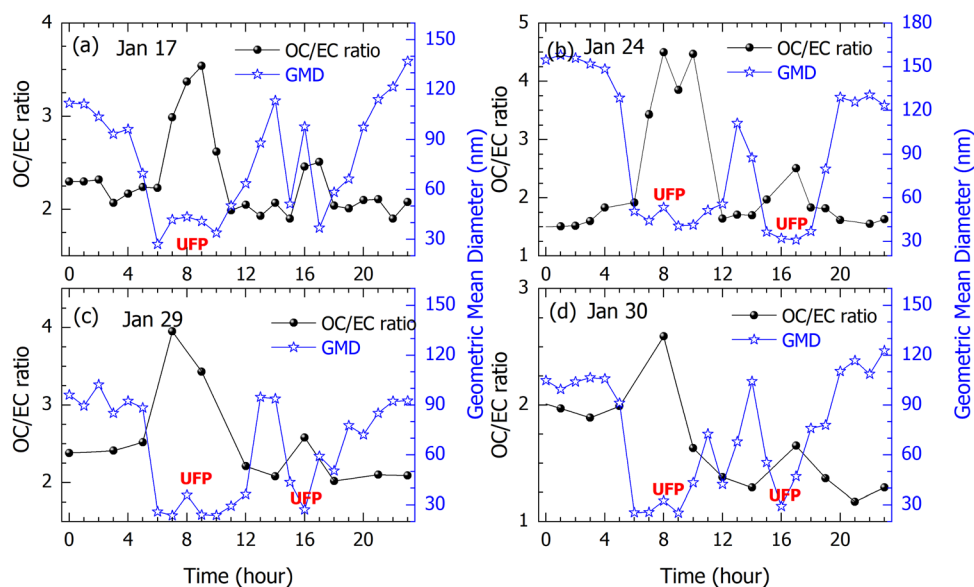


Fig. 4 Diurnal variation of the OC/EC ratio and geometric mean diameter (GMD) during the ultrafine particle (UFP) event days: (a) 17 January, (b) 24 January, (c) 29 January and (d) 30 January 2018. The location of the ship on these event days is marked in Fig. 1b.



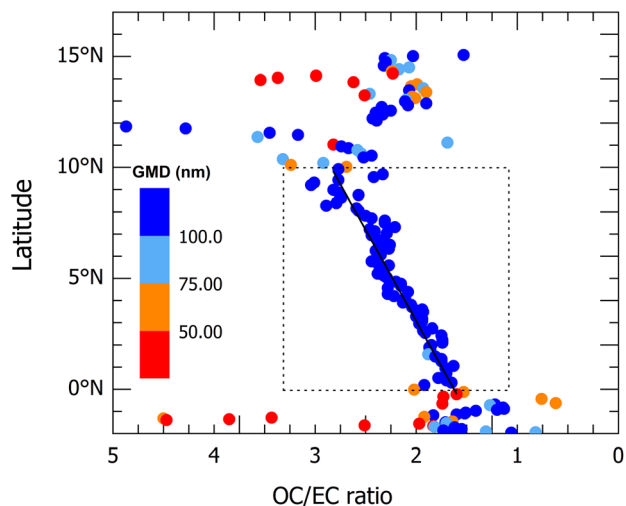


Fig. 5 Latitudinal variation of the OC/EC ratio over the Indian Ocean during ICARB-2018. Colour of the scatter indicates the geometric mean diameter (GMD) of the aerosol number size distribution.

proximity of sources and *in situ* formation of organics as shown in Fig. 3 and 4.

Fig. 6 shows the variation of OM and sulfate measured using an ACSM during the days in which ultrafine particle events were observed. An increase in the OM mass concentration (similar to that of OC in Fig. 2) was observed during the ultrafine particle events, even though these events generally do not result in a notable change in mass loading. The ultrafine particle events (UFP), which are identified by the low GMD values, were observed from 6:00 to 10:00 hours (Fig. 4 and 6). The OM mass loading showed an increasing trend from 6:00 hours and peaks at 9:00 or 10:00 hours. The estimated delay between the start of

UFP and the OM peak is almost 3–4 hours, which is attributed to the time required for the ultrafine particles to grow significant enough to influence the mass concentration. In contrast, sulfate mass loading did not show an increase during ultrafine particle events. The high values of the OM/sulfate ratio (Fig. 1e) over the equatorial Indian Ocean (open ocean) are closely related to ultrafine particle events. It should be noted that these short-term events could be averaged out in the conventional filter-based sampling.

It is seen that the EC concentration did not change during the ultrafine particle events, which discards the role of primary anthropogenic aerosols and local contamination in the observed increase in OC. The source of these ultrafine organics in the equatorial Indian Ocean is an open question, which needs dedicated field experiments to ascertain the possibility of secondary formation or the primary emission of ultrafine organics from the ocean surface layer.

Even though a higher number of ultrafine particle events and the associated increase in OC were observed over the equatorial Indian Ocean, the OC/EC ratio was lower in the equatorial Indian Ocean compared to the northern Indian Ocean. The increase in OC mass loading during the particle events in phase 2 was rather smaller compared to that of phase 1 and nucleation events were more intense during phase 1. However, the presence of a large condensation sink limits the frequency of occurrence of ultrafine particle events in phase 1. The higher values of the OC/EC ratio over the northern Indian Ocean support the higher mass of secondary aerosols formed due to condensational growth. The OC mass loading increased by almost 3 to 4  $\mu\text{g m}^{-3}$  during phase 1, whereas OC increased by 1  $\mu\text{g m}^{-3}$  over the equatorial Indian Ocean. Since the background aerosol loading was lower over the phase 2 region, the

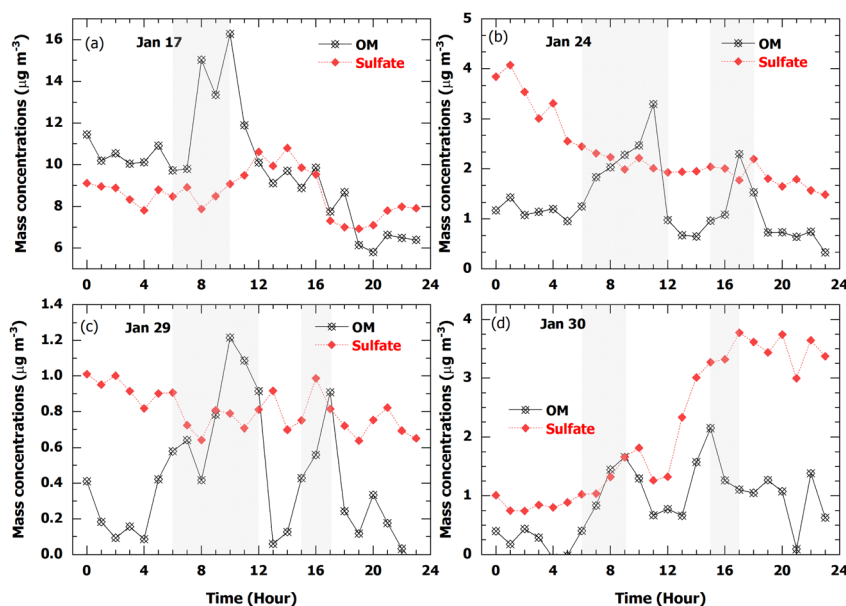


Fig. 6 Diurnal variation of organic matter (OM) and sulfate mass concentrations on (a) 17 January, (b) 24 January, (c) 29 January and (d) 30 January 2018. The ultrafine particle (UFP) event days are identified by the shaded regions.



condensation sink was weak and ultrafine particle events were more frequent over the phase 2 region.

The observation of an increase in OC associated with an ultrafine particle burst was in line with the earlier studies on the role of organic aerosols in favouring new particle formation and growth of nucleation mode aerosols. The highly oxidized organics stabilize the molecular clusters and increase the supersaturation required for new particle formation.<sup>44,45</sup> The growth rate of the ultrafine particles observed over the northern Indian Ocean during ICARB-2018 is relatively high and particles grow instantaneously to a higher size range.<sup>24</sup> So, we have observed an inverse relationship between hourly mean values of GMD and organic mass loading without much time delay. As the background aerosol number concentrations are high over the coastal Arabian Sea and continental India, organics vapours condense on the existing particles (condensation sink) instead of aerosol nucleation. However, the source identification of these precursor vapours is challenging and these vapours could be advected from the mainland or biogenic in origin.

Most of the open-ocean nucleation events (secondary formation) are associated with sulfate aerosols and there are very limited observations of organics formation, which are associated with the air–sea exchange of VOCs and their photo-oxidation. In this study, we present the increase of OM and OC aerosols during ultrafine particle events over coastal as well as remote oceanic regions using the simultaneous measurements of an SMPS, ACSM and OC-EC analyzer. As inferred from the observations, there is no evidence for anthropogenic influence on the OC enhancement over the equatorial Indian Ocean. Hence, this increase in OC during ultrafine particle events is attributed to the secondary formation of aerosols. However, the possibility of primary emission of organics from the ocean cannot be excluded.<sup>42</sup> The laboratory studies on various abiotic VOCs exchanged between the water–air surface reported the significant implications of these emissions on the aerosol nucleation and chemistry and aerosol–cloud interaction.<sup>46</sup> Since the air masses over the equatorial Indian Ocean have more marine influence than continental influence and the observed events lasted only 3 to 4 hours, we consider marine emissions (primary or secondary) to be more important than continental emissions over the phase 2 region.

### 3.3 Evolution of aerosols in the South Asian outflow

To further understand the chemical evolution of aerosols over the northern Indian Ocean, the latitudinal gradient of OM, sulfate, the OM/sulfate ratio, OC, EC and the OC/EC ratio during the first phase of the ICARB-2018 (from 15° N to 2° S, mostly between 73.5° E and 75° E) is shown in Fig. 7. The mass concentration of all the species decreases with latitude as we move away from the mainland. During phase 1, the magnitude of OC decreased almost 5-fold (15° N to 1° S) in contrast to the 3-fold decrease observed in the EC mass concentration. This difference in latitudinal gradients of OC and EC results in a small and systematic decrease in the OC/EC ratio towards the south. OM decreases at a faster rate than sulfate and EC. The OM/sulfate and OC/EC ratios also decreased with latitude,

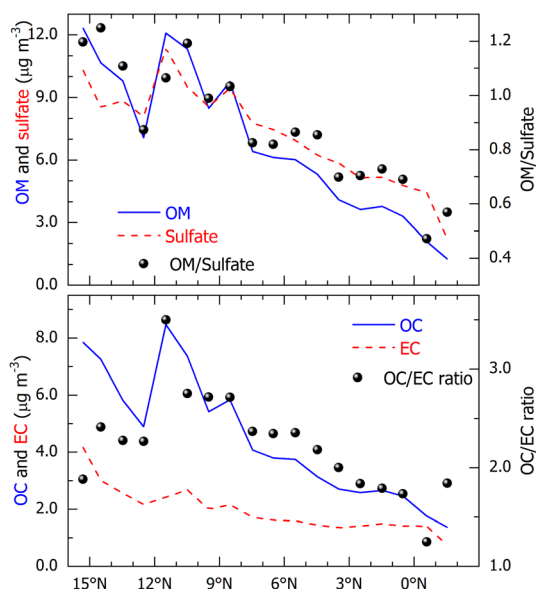


Fig. 7 Latitudinal variation of (i) OM, (ii) sulfate, (iii) the OM/sulfate ratio, (iv) OC, (v) EC and (vi) the OC/EC ratio during the phase-1 of ICARB-2018.

indicating the faster decrease in organics mass concentration (OC and OM) as the ship traversed towards the equatorial Indian Ocean. A gradual decrease in the OM/sulfate ratio and similar variation of sulfate and EC with latitude (sulfate/EC ratio varied between 2 and 4) implies the absence of additional sulfate formation over the open ocean during phase 1 of the campaign. Briefly, organic aerosols (OM and OC) showed a systematic and relatively higher decrease towards the open ocean as compared to EC and sulfate.

Hence, it is clear from Fig. 7 that the organics-rich (OM/sulfate > 1) outflow from South Asia is transformed into a sulfate-dominated outflow over the northern Indian Ocean. To further confirm the observation of gradual changes in the OM/sulfate ratio towards the open ocean, we have compiled the earlier measurements over India and the surrounding oceanic regions as shown in Fig. 8. The OM/sulfate ratio over land and ocean depicts contrasting patterns over the South Asian region. The mean OM/sulfate ratio over the Indian landmass is significantly higher (~4) than that of the northern Indian Ocean (0.6). Broadly, the OM/sulfate ratio is higher than 2 over land and less than 1 over the ocean. The OM/sulfate ratios are extremely high for urban centres like New Delhi (6.3), Kanpur (5.0), and Allahabad (5.3).<sup>4,47–51</sup> The mass concentration of OM is higher than that of sulfate over Bhubaneswar, Mahabaleswar (Western Ghats) and Manora Peak, where the OM/sulfate ratio is 1.82 (ref. 52), 4.0 (ref. 53) and 4.8 (ref. 54) respectively. Hence, the earlier studies over South Asia unambiguously highlight the organics-rich nature of the aerosol system, especially near the source regions. In contrast, the aerosol system over the northern Indian Ocean is found to be mostly sulfate-dominated (OM/sulfate ratio < 1). During the INDOEX, the OM/sulfate ratios measured onboard aircraft and the ship were 0.94 and 0.41, respectively.<sup>10</sup> Similarly, during ICARB-2006 (premonsoon),





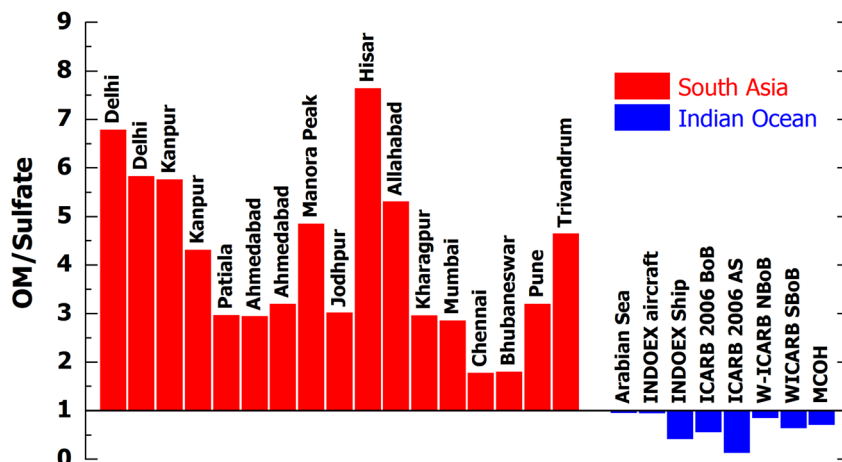


Fig. 8 Compilation of the OM/sulfate values reported for various campaigns over the northern Indian Ocean: INDOEX 1999,<sup>10,14</sup> ICARB 2006,<sup>55</sup> ICARB 2009,<sup>15</sup> and MCOH<sup>7</sup> and ICARB 2018 (present study). Values of OM/sulfate over the Indian subcontinent: Trivandrum,<sup>36</sup> Chennai,<sup>56</sup> Pune,<sup>57</sup> Mumbai,<sup>58</sup> Ahmedabad,<sup>59–61</sup> Jodhpur,<sup>61</sup> Hisar,<sup>49</sup> Patiala,<sup>5</sup> Delhi,<sup>47,50</sup> Manora Peak,<sup>54</sup> Kanpur,<sup>4,48</sup> Allahabad,<sup>49</sup> Kharagpur<sup>8</sup> and Bhubaneswar.<sup>52</sup>

values were close to 0.55 over the Bay of Bengal and 0.12 over the Arabian Sea.<sup>55</sup> Relatively higher values (0.84) were reported during ICARB-2009 (winter 2009) over the northern Bay of Bengal, which was under the influence of the IGP outflow.<sup>15</sup> The present study shows the systematic gradients in the OM/sulfate ratio, which indicate the importance of measurement location and its proximity to source regions.

This palpable flip-over from organic to sulfate dominance as the air mass traversed to the northern Indian Ocean could be attributed to the various atmospheric processes, such as the formation of sulfate from marine sources, transformation/evaporation of organics and the relative difference in the transport efficiency of aerosol species. However, we did not find an increase in sulfate mass loading during the ICARB-2018 associated with nucleation/ultrafine particle events (Fig. 6). In contrast, these ultrafine particle events contributed to the enhancement in OM and OC mass loading even over the far equatorial Indian Ocean (Fig. 3 and 4). The measurements of sulfate over the southeastern Arabian Sea are comparable to the measurements made at several land stations like Thumba and Ahmedabad.<sup>62</sup> Moreover, sulfate mass loading measured during ICARB-2018 is comparable to the earlier shipborne observations over this region. The mass fraction of sulfate during ICARB-2018 is consistent with the values (0.39–0.52) reported during the INDOEX.<sup>63</sup> During ICARB-2018, 97% of the total sulfate was non-sea salt. Earlier studies also reported 98% of total sulfate as non-sea salt and attributed diesel combustion and coal-powered thermal power plants in India and Bangladesh as the major sources.<sup>12</sup> The low values of MSA/nss-sulfate (0.003) and the high correlation of ammonium with sulfate indicate the anthropogenic origin of sulfate in the study region.<sup>13</sup> The MSA/nss-sulfate ratio remained invariant over the southeastern Arabian Sea and the equatorial Indian Ocean.<sup>13</sup> The latitudinal gradient of EC and sulfate normalized with their initial mass concentration values (at 16° N) shows an almost similar trend for EC and sulfate (0.031 and 0.038 Lat<sup>-1</sup>), and hence, sulfate/EC ratio varied between 2 and 4 (Fig. 1f). These observations

exclude the possibility of a substantial contribution from marine and transported sources to the *in situ* formation of sulfate aerosols. Hence, the present study highlights that, even in the absence of sulfate sources over the ocean, the OM/sulfate ratio is mostly less than one for the South Asian outflow due to the rapid decrease of organics. It should be noted that very low values of the OM/sulfate ratio are obvious in the presence of marine sulfate sources.

The drastic difference in the OM/sulfate ratio over continental and marine environments is further evaluated using the OC/EC ratio during ICARB-2018 (Fig. 7), where EC is mostly of continental origin and chemically inert compared to sulfate aerosols. Since EC does not have prominent sources over the ocean, the systematic decrease observed in the OC/EC ratio is attributed to the depletion of OC during long-range transport. This again supports the low OM/sulfate ratio over the northern and equatorial Indian Ocean. As shown in Fig. 9, the earlier measurements over the Indian landmass showed a high OC/EC ratio ( $6 \pm 2$ ), which indicates the dominance of biomass/biofuel burning over South Asia.<sup>4,8,35,47,50,64–66</sup> However, the OC/EC ratio measurements over the northern Indian Ocean ( $2.8 \pm 1.2$ ) depicted relatively lower OC/EC ratios compared to the land region.<sup>7,10,14,15,55</sup> Even though organics have emission sources over the equatorial Indian Ocean as seen during ultrafine particle events (Fig. 3, 4 and 6), the decrease in OM and OC mass loading is far higher than that of marine production, which resulted in a larger latitudinal gradient in OM and OC compared to sulfate and EC (Fig. 7) over the open ocean. The latitudinal dependence of OC/Sulfate, OC/EC and sulfate/EC over the Bay of Bengal, which is under the influence of the outflow from the Indo-Gangetic Plain, was investigated using measurements by Srinivas *et al.*<sup>15</sup> As shown in supplementary Fig. S1,<sup>†</sup> measurements over the Bay of Bengal during ICARB-2009 also depict a systematic decrease in the OC/EC ratio and OC/nss-sulfate with latitude. Moreover, there is no latitudinal trend in the nss-sulfate/EC ratio. As the air mass pattern was continental over the northern and southern Bay of Bengal, the



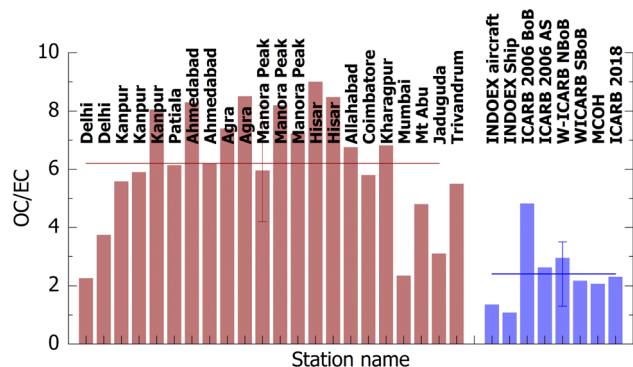


Fig. 9 Compilation of the OC/EC ratio reported over South Asia and the surrounding oceanic regions. Measurement over land sites [Delhi,<sup>47,50</sup> Kanpur,<sup>4,49,65</sup> Patiala,<sup>5</sup> Ahmedabad,<sup>59,60,67</sup> Agra,<sup>68,69</sup> Manora Peak,<sup>54,66</sup> Hisar,<sup>49,66</sup> Allahabad,<sup>49</sup> Coimbatore,<sup>35</sup> Kharagpur,<sup>8</sup> Mumbai,<sup>58</sup> Mt. Abu,<sup>70</sup> Jaduguda,<sup>6</sup> and Trivandrum<sup>36</sup>] and during ocean experiments [INDOEX,<sup>10,14</sup> ICARB-2006,<sup>55</sup> W-ICARB,<sup>9,15</sup> and MCOH<sup>7</sup>] is shown in a different colour.

low values of the OC/EC ratio and OC/nss-sulfate over the southern Bay of Bengal are attributed to the ageing of the air mass during long-range transport from the mainland. Hence, the earlier measurements over the Bay of Bengal during winter 2009 also support the loss of organics due to ageing during long-range transport.

Generally, the concentration of the continental aerosols decrease as we move towards the open ocean (equatorial Indian Ocean) due to removal processes.<sup>3,11,41</sup> Apart from wet and dry deposition, organics has significant loss processes initiated by oxidization (heterogeneous and aqueous phases) and photolysis followed by fragmentation and evaporation.<sup>22</sup> Several studies have reported a decrease in the mass loading of secondary organics due to oxidation and photolysis, which fragment organics into smaller fragments with higher volatility. This is mostly valid for an aged oxygenated organic aerosol system in the outflow regions.<sup>21</sup> The SOA mass loss due to UV photolysis and oxidation is considered as a potential removal mechanism for the organics as shown by the modelling studies, where the SOA mass decreased 40–60% for an atmospheric ageing of 10 days.<sup>71</sup> Photodegradation and fragmentation reduce the lifetime of organic aerosols to shorter scales and thus decrease the efficiency of their transport to longer distances. Hence, (i) the low OC/EC ratio observed over the equatorial Indian Ocean, (ii) a systematic gradient in the OC/EC ratio and (iii) gradients in the OM/sulfate ratio towards the open ocean could be attributed to the loss of organic aerosols due to photodegradation and fragmentation during long-range transport. In contrast to the loss of SOA mass due to fragmentation and increased volatility, the functionalization of organic aerosols due to ageing results in the increase of SOA mass loading, which is less prominent for highly oxygenated organics. Using an explicit gas-phase chemistry model, studies have reported dilution-induced evaporation of organics for the outflow from a Mexican city, which partly compensates for the increase in the secondary organic aerosol mass due to photochemical oxidation processes.<sup>71</sup> During

ICARB-2018, loss of organics due to photochemical ageing overwhelms the increase in organics mass loading during the ultrafine particle events over the equatorial Indian Ocean. This loss will result in the change in volatility of organic aerosols and thus affect the hygroscopicity and cloud condensation nuclei properties in the far oceanic regions.

Several studies have identified the loss of volatile vapours from thermodynamically active primary organic compounds due to oxidation as a potential pathway for the formation of secondary organic aerosols.<sup>23,71,72</sup> Possible oxidation of primary organics due to the heterogeneous reactions involving the other species (such as OH, O<sub>3</sub>, NO<sub>3</sub>, etc.) during long-range transport can easily result in their volatilization. Primary organic aerosols (POAs) evaporate due to the dilution under ambient conditions and the subsequent photooxidation of the gas phase precursors could repartition as secondary organics.<sup>72</sup> The presence of a small amount of hydrophobic organics (like polycyclic aromatic hydrocarbon) in the SOA reduces the evaporation rate significantly.<sup>73</sup> Based on the measurements made from the island location (MCOH) in the equatorial Indian Ocean, studies attributed the photochemical ageing during long-range transport to the large difference in the absorption properties of brown carbon (or light absorbing OC) observed over the source (IGP) to receptor (MCOH) regions.<sup>12</sup> Hence, the photochemical ageing of organics has implications not only for the mass budget but also for radiation absorption and cloud condensation nuclei (CCN).

Despite several studies reporting a significant contribution of secondary organics to the total organic aerosols,<sup>18</sup> direct observations of an increase in OC and OM during the ultrafine particle events are rather nonexistent over the South Asian region, which is probably due to the coarse temporal resolution (12 to 24 hours) of earlier filter-based offline OC measurements. Condensation of organic vapours onto newly formed particles contributes significantly to ultrafine particle growth and thus the number concentration of CCN. The high growth rate (~15–50 nm h<sup>-1</sup>) of ultrafine particles during ICARB-2018 was attributed to the presence of organics,<sup>24</sup> where inorganics (like sulfate) alone do not account for the high growth rate of ultrafine particles. The present study shows an enhancement in the OC concentration and hence the OC/EC ratio during the ultrafine particle events; however, the source of these organic vapours is still uncertain (anthropogenic or ocean biogenic). Recent laboratory data and modelling studies suggest that highly oxidized organic vapours with very low volatility condense on the newly formed particles and contribute to the rapid growth of these particles to CCN-relevant size ranges.<sup>44,45,74</sup> As a result, the high growth rate of fine particles and the associated increase in organic mass loading have implications on CCN activation efficiency over the region.<sup>45</sup> In addition, the loss of organics in the continental outflow and the associated change in chemical composition have significant implications on CCN activation and the aerosol–climate interaction over South Asia. Furthermore, the organics speciation and evaporation of different components need to be investigated in the light of the increase in organics mass loading observed during ultrafine particle events, which forms the scope of a future study.



## 4 Conclusions

The characterization of the South Asian outflow over the northern Indian Ocean was carried out using the measurements of aerosol chemical composition as a part of shipborne experiments under the ICARB experiment during winter 2018. The major highlights of these high-resolution measurements are

- The mass concentration of OC, EC, OM and sulfate showed higher values over the northern Indian Ocean ( $OC = 4.8 \pm 2.1 \mu\text{g m}^{-3}$  and  $EC = 2.0 \pm 0.6 \mu\text{g m}^{-3}$ ,  $OM = 7.3 \pm 3.0 \mu\text{g m}^{-3}$ ) compared to the equatorial Indian Ocean ( $OC = 1.20 \pm 0.50 \mu\text{g m}^{-3}$  and  $EC = 0.82 \pm 0.53 \mu\text{g m}^{-3}$ ,  $OM = 2.4 \pm 3.0 \mu\text{g m}^{-3}$ ). The OC/EC ratio and OM/sulfate ratio also showed a systematic decrease towards the equatorial Indian Ocean, which indicates the species-specific evolution of the South Asian outflow over oceans far away from the source regions.

- An episodic increase in OC and OM mass concentrations was observed during the ultrafine particle events in the early morning and evening hours over the southeastern Arabian Sea and equatorial Indian Ocean. Since the air mass back trajectories and EC values did not support the influence from anthropogenic sources, the observed association between OC and ultrafine particle events is attributed to the marine sources of organic aerosols.

- The latitudinal gradient of EC and sulfate normalized with their initial mass concentration values (at  $16^\circ\text{N}$ ) shows an almost similar trend for EC and sulfate ( $0.031$  and  $0.038 \text{ Lat}^{-1}$ ). The rapid decrease of OM with latitude ( $0.05 \text{ Lat}^{-1}$ ) towards the open ocean, which is higher than that for sulfate and EC, indicates the possible loss of organics during long-range transport, which might be due to ageing and photo-degradation processes. The relative dominance of sulfate ( $OM/sulfate < 1$ ) over the northern Indian Ocean also supports the observation of loss of organics (*via* ageing, photochemical oxidation and dilution) rather than the presence of marine sources for sulfate.

- Regional synthesis of earlier observations of OC (or OM) over South Asia and surrounding oceanic regions showed the dominance of organics over the Indian mainland ( $OM/sulfate \text{ ratio} \sim 4$ ), whereas sulfate dominated over the Indian Ocean ( $OM/sulfate \text{ ratio} \sim 0.6$ ) during the winter. Changes in the OC/EC ratio over South Asia ( $OC/EC \sim 6$ ) and the Indian Ocean ( $OC/EC \text{ ratio} \sim 2.8$ ) also support the variation of the OM/sulfate ratio.

Based on the observations made during ICARB-2018, more studies on the formation of organics in the marine environment and its evolution during long-range transport need to be carried out in the future using high-resolution mass spectrometer measurements.

## Author contributions

SSB and VSN conceptualized the experiment. VJ, VSN, SKK and MMG were involved in the data collection. SKK, TCA and VSN analyzed the data and wrote the manuscript. SSB review-edited the draft.

## Conflicts of interest

The authors declare that they have no known competing financial interests or personal relationships that could have appeared to influence the work reported in this paper.

## Acknowledgements

The ICARB-2018 experiment was carried out under the ISRO Geosphere-Biosphere Programme. The authors acknowledge the National Centre for Polar and Ocean Research (NCPOR) of the Ministry of Earth Sciences for providing the shipboard facilities onboard ORV Sagar Kanya. Nair, V. S. acknowledges the Science and Engineering Research Board for the Swarna-Jayanti Fellowship (SB/SJF/2020-21/04). We acknowledge NOAA ARL for providing the Hybrid Single-Particle Lagrangian Integrated Trajectory (HYSPPLIT) transport and dispersion model used in this study.

## Notes and references

- 1 C. Bharali, V. S. Nair, L. Chutia and S. S. Babu, *J. Geophys. Res.: Atmos.*, 2019, **124**, 4141–4157.
- 2 V. S. Nair, K. K. Moorthy, D. P. Alappattu, P. K. Kunhikrishnan, S. George, P. R. Nair, S. S. Babu, B. Abish, S. K. Satheesh, S. N. Tripathi, K. Niranjan, B. L. Madhavan, V. Srikant, C. B. S. Dutt, K. V. S. Badarinath and R. R. Reddy, *J. Geophys. Res.: Atmos.*, 2007, **112**, 2006JD008099.
- 3 V. Ramanathan, P. J. Crutzen, J. Lelieveld, A. P. Mitra, D. Althausen, J. Anderson, M. O. Andreae, W. Cantrell, G. R. Cass, C. E. Chung, A. D. Clarke, J. A. Coakley, W. D. Collins, W. C. Conant, F. Dulac, J. Heintzenberg, A. J. Heymsfield, B. Holben, S. Howell, J. Hudson, A. Jayaraman, J. T. Kiehl, T. N. Krishnamurti, D. Lubin, G. McFarquhar, T. Novakov, J. A. Ogren, I. A. Podgorny, K. Prather, K. Priestley, J. M. Prospero, P. K. Quinn, K. Rajeev, P. Rasch, S. Rupert, R. Sadourny, S. K. Satheesh, G. E. Shaw, P. Sheridan and F. P. J. Valero, *J. Geophys. Res.: Atmos.*, 2001, **106**, 28371–28398.
- 4 K. Ram and M. Sarin, *Atmos. Environ.*, 2011, **45**, 460–468.
- 5 N. Rastogi, A. Singh, M. Sarin and D. Singh, *Atmos. Environ.*, 2016, **125**, 396–403.
- 6 K. Ram and M. Sarin, *J. Aerosol Sci.*, 2010, **41**, 88–98.
- 7 K. Budhavant, S. Bikkina, A. Andersson, E. Asmi, J. Backman, J. Kesti, H. Zahid, S. K. Satheesh and O. Gustafsson, *Tellus B*, 2018, **70**, 1–15.
- 8 B. Srinivas and M. Sarin, *Sci. Total Environ.*, 2014, **487**, 196–205.
- 9 B. Srinivas and M. M. Sarin, *Environ. Res. Lett.*, 2013, **8**, 044042.
- 10 O. L. Mayol-Bracero, *J. Geophys. Res.*, 2002, **107**, 8030.
- 11 V. S. Nair, S. S. Babu and K. K. Moorthy, *J. Geophys. Res.*, 2008, **113**, D15208.
- 12 S. Dasari, A. Andersson, S. Bikkina, H. Holmstrand, K. Budhavant, S. Satheesh, E. Asmi, J. Kesti, J. Backman,



- A. Salam, D. S. Bisht, S. Tiwari, Z. Hameed and O. Gustafsson, *Sci. Adv.*, 2019, **5**, eaau8066.
- 13 A. Aswini, P. Hegde, S. Aryasree, I. A. Girach and P. R. Nair, *Sci. Total Environ.*, 2020, **712**, 135214.
- 14 W. P. Ball, *J. Geophys. Res.*, 2003, **108**, 8001.
- 15 B. Srinivas, A. Kumar, M. M. Sarin and A. K. Sudheer, *Atmos. Chem. Phys. Discuss.*, 2011, **11**, 20667–20711.
- 16 D. V. Spracklen, J. L. Jimenez, K. S. Carslaw, D. R. Worsnop, M. J. Evans, G. W. Mann, Q. Zhang, M. R. Canagaratna, J. Allan, H. Coe, G. McFiggans, A. Rap and P. Forster, *Atmos. Chem. Phys.*, 2011, **11**, 12109–12136.
- 17 B. R. Bzdek, M. J. Lawler, A. J. Horan, M. R. Pennington, J. W. DePalma, J. Zhao, J. N. Smith and M. V. Johnston, *Geophys. Res. Lett.*, 2014, **41**, 6045–6054.
- 18 I. Riipinen, J. R. Pierce, T. Yli-Juuti, T. Nieminen, S. Häkkinen, M. Ehn, H. Junninen, K. Lehtipalo, T. Petäjä, J. Slowik, R. Chang, N. C. Shantz, J. Abbatt, W. R. Leaitch, V.-M. Kerminen, D. R. Worsnop, S. N. Pandis, N. M. Donahue and M. Kulmala, *Atmos. Chem. Phys.*, 2011, **11**, 3865–3878.
- 19 M. Shiraiwa, Y. Li, A. P. Tsimpidi, V. A. Karydis, T. Berkemeier, S. N. Pandis, J. Lelieveld, T. Koop and U. Pöschl, *Nat. Commun.*, 2017, **8**, 15002.
- 20 A. Hodzic, P. S. Kasibhatla, D. S. Jo, C. D. Cappa, J. L. Jimenez, S. Madronich and R. J. Park, *Atmos. Chem. Phys.*, 2016, **16**, 7917–7941.
- 21 J. H. Kroll, J. D. Smith, D. L. Che, S. H. Kessler, D. R. Worsnop and K. R. Wilson, *Phys. Chem. Chem. Phys.*, 2009, **11**, 8005.
- 22 K. T. Malecha and S. A. Nizkorodov, *Environ. Sci. Technol.*, 2016, **50**, 9990–9997.
- 23 A. A. Presto, M. A. Miracolo, J. H. Kroll, D. R. Worsnop, A. L. Robinson and N. M. Donahue, *Environ. Sci. Technol.*, 2009, **43**, 4744–4749.
- 24 S. K. Kompalli, V. S. Nair, V. Jayachandran, M. M. Gogoi and S. S. Babu, *Atmos. Environ.*, 2020, **238**, 117719.
- 25 M. Canagaratna, J. Jayne, J. Jimenez, J. Allan, M. Alfarra, Q. Zhang, T. Onasch, F. Drewnick, H. Coe, A. Middlebrook, A. Delia, L. Williams, A. Trimborn, M. Northway, P. DeCarlo, C. Kolb, P. Davidovits and D. Worsnop, *Mass Spectrom. Rev.*, 2007, **26**, 185–222.
- 26 V. Crenn, J. Sciare, P. L. Croteau, S. Verlhac, R. Fröhlich, C. A. Belis, W. Aas, M. Äijälä, A. Alastuey, B. Artiñano, D. Baisnée, N. Bonnaire, M. Bressi, M. Canagaratna, F. Canonaco, C. Carbone, F. Cavalli, E. Coz, M. J. Cubison, J. K. Esser-Gietl, D. C. Green, V. Gros, L. Heikkinen, H. Herrmann, C. Lunder, M. C. Minguillón, G. Močnik, C. D. O'Dowd, J. Ovadnevaite, J.-E. Petit, E. Petralia, L. Poulain, M. Priestman, V. Riffault, A. Ripoll, R. Sarda-Estève, J. G. Slowik, A. Setyan, A. Wiedensohler, U. Baltensperger, A. S. H. Prévôt, J. T. Jayne and O. Favez, *Atmos. Meas. Tech.*, 2015, **8**, 5063–5087.
- 27 A. M. Middlebrook, R. Bahreini, J. L. Jimenez and M. R. Canagaratna, *Aerosol Sci. Technol.*, 2012, **46**, 258–271.
- 28 N. L. Ng, S. C. Herndon, A. Trimborn, M. R. Canagaratna, P. L. Croteau, T. B. Onasch, D. Sueper, D. R. Worsnop, Q. Zhang, Y. L. Sun and J. T. Jayne, *Aerosol Sci. Technol.*, 2011, **45**, 780–794.
- 29 Y. Sun, Z. Wang, H. Dong, T. Yang, J. Li, X. Pan, P. Chen and J. T. Jayne, *Atmos. Environ.*, 2012, **51**, 250–259.
- 30 W. Hu, P. Campuzano-Jost, D. A. Day, P. Croteau, M. R. Canagaratna, J. T. Jayne, D. R. Worsnop and J. L. Jimenez, *Atmos. Meas. Tech.*, 2017, **10**, 2897–2921.
- 31 M. E. Birch and R. A. Cary, *Aerosol Sci. Technol.*, 1996, **25**, 221–241.
- 32 J. J. Bauer, X.-Y. Yu, R. Cary, N. Laulainen and C. Berkowitz, *J. Air Waste Manage. Assoc.*, 2009, **59**, 826–833.
- 33 A. Karanasiou, P. Panteliadis, N. Pérez, M. C. Minguillón, M. Pandolfi, G. Titos, M. Viana, T. Moreno, X. Querol and A. Alastuey, *Sci. Total Environ.*, 2020, **747**, 141266.
- 34 S. C. Wang and R. C. Flagan, *Aerosol Sci. Technol.*, 1990, **13**, 230–240.
- 35 A. Aswini, P. Hegde and P. R. Nair, *Atmos. Res.*, 2018, **199**, 40–53.
- 36 P. Hegde and K. Kawamura, *Arch. Environ. Contam. Toxicol.*, 2017, **73**, 456–473.
- 37 B. Kumar, A. Chakraborty, S. N. Tripathi and D. Bhattu, *Environ. Sci.: Processes Impacts*, 2016, **18**, 1285–1296.
- 38 P. Rajput, *Aerosol Science and Engineering*, 2018, **2**, 153–164.
- 39 B. J. Turpin and H.-J. Lim, *Aerosol Sci. Technol.*, 2001, **35**, 602–610.
- 40 J. Brooks, J. D. Allan, P. I. Williams, D. Liu, C. Fox, J. Haywood, J. M. Langridge, E. J. Highwood, S. K. Kompalli, D. O'Sullivan, S. S. Babu, S. K. Satheesh, A. G. Turner and H. Coe, *Atmos. Chem. Phys.*, 2019, **19**, 5615–5634.
- 41 I. Girach, V. S. Nair, S. S. Babu and P. R. Nair, *Atmos. Environ.*, 2014, **94**, 508–517.
- 42 S. Huang, Z. Wu, L. Poulain, M. van Pinxteren, M. Merkel, D. Assmann, H. Herrmann and A. Wiedensohler, *Atmos. Chem. Phys.*, 2018, **18**, 18043–18062.
- 43 A. R. Aswini, P. Hegde, S. K. R. Boreddy and P. R. Nair, *ACS Earth Space Chem.*, 2022, **6**, 56–72.
- 44 N. M. Donahue, I. K. Ortega, W. Chuang, I. Riipinen, F. Riccobono, S. Schobesberger, J. Dommen, U. Baltensperger, M. Kulmala, D. R. Worsnop and H. Vehkamäki, *Faraday Discuss.*, 2013, **165**, 91.
- 45 C. Mohr, J. A. Thornton, A. Heitto, F. D. Lopez-Hilfiker, A. Lutz, I. Riipinen, J. Hong, N. M. Donahue, M. Hallquist, T. Petäjä, M. Kulmala and T. Yli-Juuti, *Nat. Commun.*, 2019, **10**, 4442.
- 46 G. A. Novak and T. H. Bertram, *Acc. Chem. Res.*, 2020, **53**, 1014–1023.
- 47 P. Pant, A. Shukla, S. D. Kohl, J. C. Chow, J. G. Watson and R. M. Harrison, *Atmos. Environ.*, 2015, **109**, 178–189.
- 48 K. Ram, M. M. Sarin and S. N. Tripathi, *Environ. Sci. Technol.*, 2012, **46**, 686–695.
- 49 K. Ram, M. Sarin, A. Sudheer and R. Rengarajan, *Aerosol Air Qual. Res.*, 2012, **12**, 359–370.
- 50 S. Sharma, T. Mandal, M. Saxena, Rashmi, A. Sharma, A. Datta and T. Saud, *J. Atmos. Sol.-Terr. Phys.*, 2014, **113**, 10–22.





- 51 S. Tiwari, U. Dumka, D. Kaskaoutis, K. Ram, A. Panicker, M. Srivastava, S. Tiwari, S. Attri, V. Soni and A. Pandey, *Atmos. Environ.*, 2016, **125**, 437–449.
- 52 S. K. Kompalli, S. N. Suresh Babu, S. K. Satheesh, K. Krishna Moorthy, T. Das, R. Boopathy, D. Liu, E. Darbyshire, J. D. Allan, J. Brooks, M. J. Flynn and H. Coe, *Atmos. Chem. Phys.*, 2020, **20**, 3965–3985.
- 53 V. Singla, S. Mukherjee, P. Safai, G. Meena, K. Dani and G. Pandithurai, *Atmos. Environ.*, 2017, **158**, 148–159.
- 54 K. Ram, M. M. Sarin and P. Hegde, *Atmos. Chem. Phys.*, 2010, **10**, 11791–11803.
- 55 A. Kumar, A. K. Sudheer and M. M. Sarin, *J. Earth Syst. Sci.*, 2008, **117**, 325–332.
- 56 C. M. Pavuluri, K. Kawamura, S. G. Aggarwal and T. Swaminathan, *Atmos. Chem. Phys.*, 2011, **11**, 8215–8230.
- 57 R. D. Gawhane, P. S. P. Rao, K. B. Budhavant, V. Waghmare, D. C. Meshram and P. D. Safai, *Environ. Sci. Pollut. Res.*, 2017, **24**, 21065–21072.
- 58 S. G. Aggarwal, K. Kawamura, G. S. Umarji, E. Tachibana, R. S. Patil and P. K. Gupta, *Atmos. Chem. Phys.*, 2013, **13**, 4667–4680.
- 59 R. Rengarajan, A. Sudheer and M. Sarin, *Atmos. Environ.*, 2011, **45**, 1940–1945.
- 60 R. Rengarajan, A. Sudheer and M. Sarin, *Atmos. Res.*, 2011, **102**, 420–431.
- 61 A. Sudheer, M. Aslam, M. Upadhyay, R. Rengarajan, R. Bhushan, J. Rathore, S. Singh and S. Kumar, *Atmos. Res.*, 2016, **178–179**, 268–278.
- 62 P. R. Nair, S. K. George, S. Sunilkumar, K. Parameswaran, S. Jacob and A. Abraham, *Atmos. Environ.*, 2006, **40**, 6477–6493.
- 63 A. D. Clarke, *J. Geophys. Res.*, 2002, **107**, 8033.
- 64 S. A. Guazzotti, *J. Geophys. Res.*, 2003, **108**, 4485.
- 65 K. Ram, S. Tripathi, M. Sarin and D. Bhattu, *Atmos. Environ.*, 2014, **89**, 655–663.
- 66 R. Rengarajan, M. M. Sarin and A. K. Sudheer, *J. Geophys. Res.*, 2007, **112**, D21307.
- 67 N. Rastogi and M. Sarin, *Atmos. Environ.*, 2009, **43**, 3481–3488.
- 68 T. Pachauri, A. Satsangi, V. Singla, A. Lakhani and K. M. Kumari, *Aerosol Air Qual. Res.*, 2013, **13**, 977–991.
- 69 A. Satsangi, T. Pachauri, V. Singla, A. Lakhani and K. M. Kumari, *Atmos. Res.*, 2012, **113**, 13–21.
- 70 K. Ram, M. Sarin and P. Hegde, *Atmos. Environ.*, 2008, **42**, 6785–6796.
- 71 J. Lee-Taylor, S. Madronich, B. Aumont, A. Baker, M. Camredon, A. Hodzic, G. S. Tyndall, E. Apel and R. A. Zaveri, *Atmos. Chem. Phys.*, 2011, **11**, 13219–13241.
- 72 A. L. Robinson, N. M. Donahue, M. K. Shrivastava, E. A. Weitkamp, A. M. Sage, A. P. Grieshop, T. E. Lane, J. R. Pierce and S. N. Pandis, *Science*, 2007, **315**, 1259–1262.
- 73 A. Zelenyuk, D. Imre, J. Beránek, E. Abramson, J. Wilson and M. Shrivastava, *Environ. Sci. Technol.*, 2012, **46**, 12459–12466.
- 74 R. A. Zaveri, J. E. Shilling, A. Zelenyuk, M. A. Zawadowicz, K. Suski, S. China, D. M. Bell, D. Veghte and A. Laskin, *Environ. Sci. Technol.*, 2020, **54**, 2595–2605.

